Article ID: 1006-8775(2007) 02-0120-12

THE DYNAMICAL ANALYSIS OF THE STRUCTURE OF B MESO-SCALE DOUBLE RAINBANDS IN MEIYU FRONT

WANG Chun-ming (王春明), WANG Yuan (王　元), WU Rong-sheng (伍荣生)

(Key Laboratory for Mesoscale Severe Weather of Ministry of Education, Nanjing University, Nanjing 210093 China)

ABSTRACT: In this paper, an idealized perturbation following the "surge-flow conceptual model" for typical Meiyu frontal structure is designed to explain the β meso-scale structure of rainbands in the Meiyu front using a non-hydrostatic, full-compressible storm-scale model including multi-phase microphysical parameterization. In addition, sensitivity numerical experiment on the vertical distribution of the ambient meridional wind is conducted to investigate the generation mechanism of β meso-scale double rainbands. The results of numerical experiments show that the cool and dry downdraft invading strengthened by the environmental aloft northerly wind plays a very important role to the generation and maintenance of the β meso-scale double rainbands. Moreover, the intensity and scale of the dry and cool downdraft invading are related to the intensity of the second circumfluence induced by mass adjustment when the acceleration of the westerly jet aloft occurs.

Key words: β meso-scale rainbands in Meiyu front; dry and cool downdraft; acceleration of westerly jet aloft

CLC number: P441 **Document code:** A

1 INTRODUCTION

Many previous researches showed that the Meiyu in Yangtze River was caused by the warm-moist monsoon flow interacting with the transformed cold air mass during steady synoptic circumfluence position (Tao et al.[1], Tao[2], Zhang[3], Li et al.[4]). Among others, the "East China Meso-scale Synoptic Experiments" (Zhang[3]) obtained many observational synoptic and meso-scale data about Meiyu. It was these observational data that firstly provided the facets of Meiyu meso-scale structure for the subsequent studies before 1990s. The Meiyu front is a synoptic scale quasi-stationary cloud band oriented in the northeast-southwest direction that frequently embeds with cumulonimbus clusters. These cumulonimbus clusters often appear as meso-scale heavy rainstorm rainbands. Moreover, the meso-scale double rainbands structure occurs frequently, such as those observed during June 24 – 27 in 1981 and those during June 23 – 26 in 1983 (Zhang[3]). Recently, the β meso-scale double rainbands structure is also observed in radar analysis (Fig.1) during the Meiyu period.

It is worth noticing that double rainbands are observed significantly in the 1999 Meiyu period, which caused a huge disaster. The observations of day rainfall of July 23, 1999 show that there are two rainbands orientated from Southwest to Northeast along 30°N – 32°N and 33°N – 35°N respectively, both of which parallel the Meiyu frontal zone (see Fig. 2, the Meiyu frontal zone is denoted with the interface between the 0°K and -4°K contours of perturbation potential temperature on 850hPa). And the southern rainband is stronger than the northern one. Moreover, the β meso-scale double rainbands structures are more evidently showed in the moving average of 3-h rainfall (Fig. 3a – d). In addition, the mean scale of each rainband is about 200 – 300 km in length and 100 – 150 km in width, while the mean distance between the β meso-scale rainbands is about 100 – 150 km. The combination of the β meso-scale double rainbands generally means the occurrence of heavy rainfall and flooding disaster.

The inhomogeneous distribution of severe

Received date: 2007-03-08; **revised date:** 2007-09-05

Foundation item: State Key Basic Program (Project 973, 2004CB18301), Doctorate-Supervisor Foundation, MOE under Grant (20050284035), and Project of Natural Science Foundation of Jiangsu Province (BK99020, BK2005081)

Biography: WANG Chun-ming (1970 -), male, native from Heilongjiang Province, Ph.D. candidate, associate professor and guest researcher at Nanjing University, mainly undertaking the study on mesoscale numerical simulation.

E-mail of corresponding author: yuanasm@nju.edu.cn

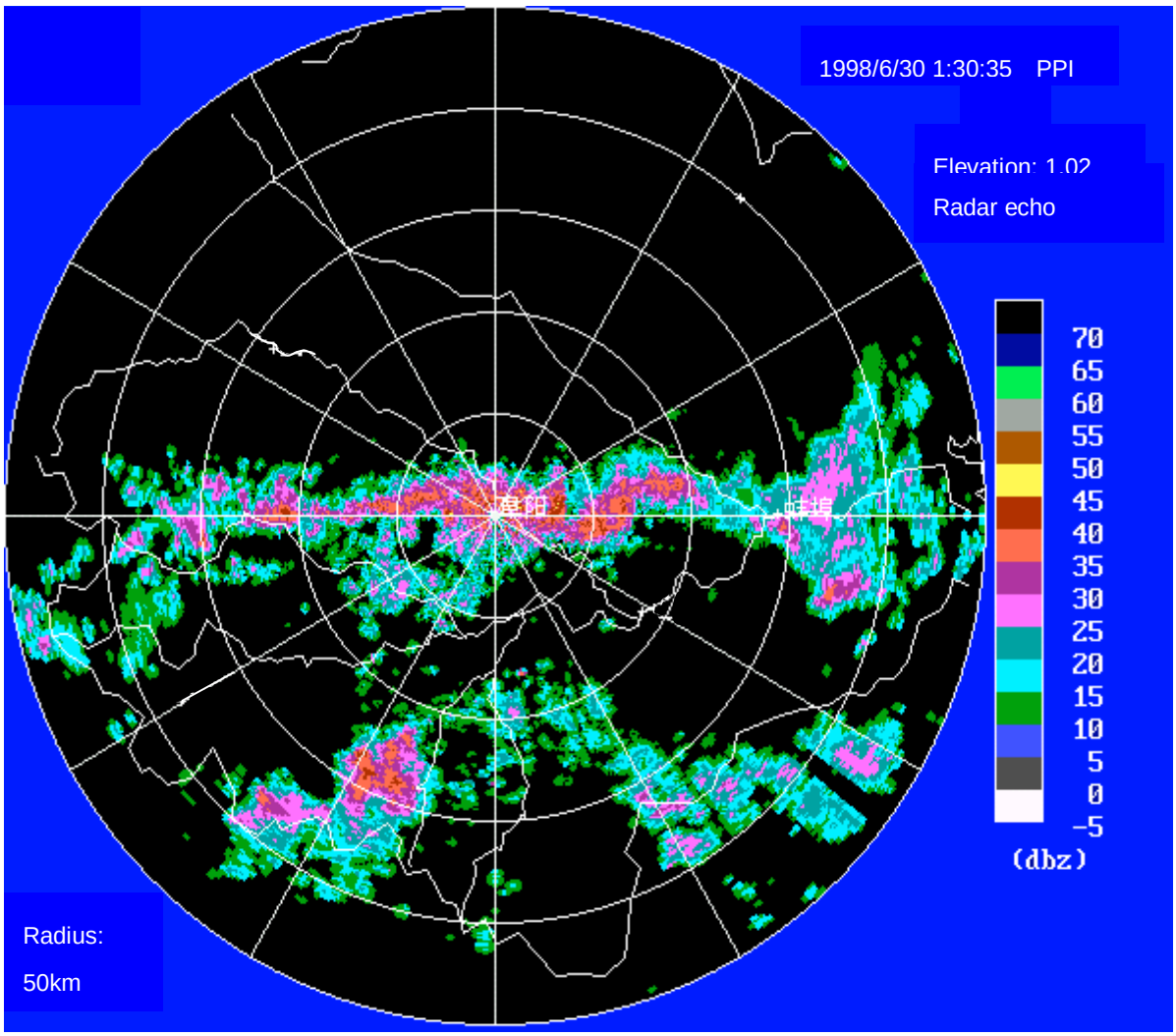

Fig 1 The meso-scale rainbands structure in Radar observation at Fuyang in An-Hui province, JUN 30,1998.

rainstorm along the Meiyu front has been extensively studied (Tao et al.[5], Bei[6]), while there is indeed no conceptual model to explain why the inhomogeneous distribution of heavy rainfall bands is perpendicular to the Meiyu frontal zone, and the generation and maintenance mechanism behind the β meso-scale double rainbands. Since this kind of β meso-scale rainbands are often unable and therefore neglected in conventional synoptic analysis, and the combination of the double rainbands generally means the occurrence of heavy rainfall, it is of great interest to investigate the generation and maintenance mechanism of the β meso-scale double rainbands, especially for localized heavy precipitation.

In this paper, an idealized perturbation following the "surge-flow conceptual model" for typical Meiyu frontal structure (Wu[7]) is designed that is constrained within the moist thermal-wind equilibrium limitation. Then, the sensitivity experiments of vertical distribution of the environmental meridional velocity are numerically implemented in order to discuss the generation and maintenance mechanism of the β meso-scale double rainbands being perpendicular to the Meiyu front.

2 BASIC METHOD AND THE IDEAL PERTURBATION DESIGN DESCRIPTIONS

2.1 *Model descriptions*

The numerical model used in this study is a three-dimensional nonhydrostatic storm-scale model, the Advanced Regional Prediction System (ARPS), which is developed from the cloud model (Klemp and Whilhelmson[8]) to include ice microphysics at the Center for Analysis and Prediction of Storm (CAPS), University of Oklahoma (OU), the United States. The model uses a complete set of fully compressible equations and parameterized cloud microphysics to

predict the horizontal and vertical wind fields, potential temperature, pressure, water vapor, cloud water, rain, ice, snow and hail (see Xue et al.[9]).

In the present experiments, the grid resolution is 20 km horizontally and 500 m vertically. The domain is configured to use a 43×103 horizontal grid with 33 levels in the vertical, which yields a simulation domain with 800 km in the zonal (parallel to the frontal zone)

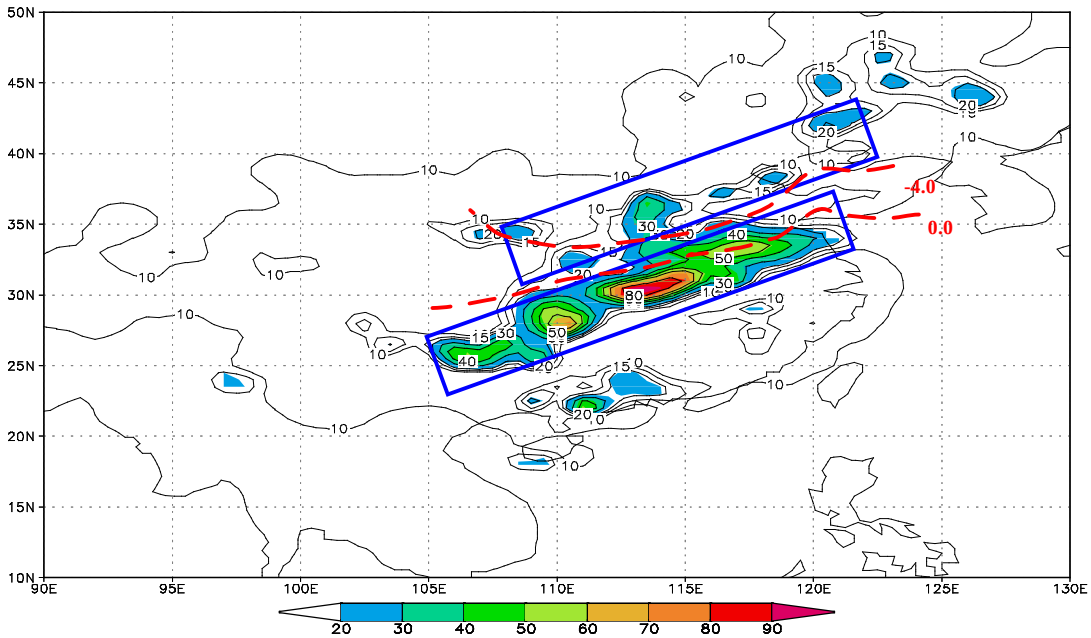

Fig 2 The observation of day rainfall JUN 23 in 1999. The shaded area denotes where the day rainfall is above 20mm, the rectangle zone denotes the rainbands, and the dashed lines denote the front zone on 850hPa.

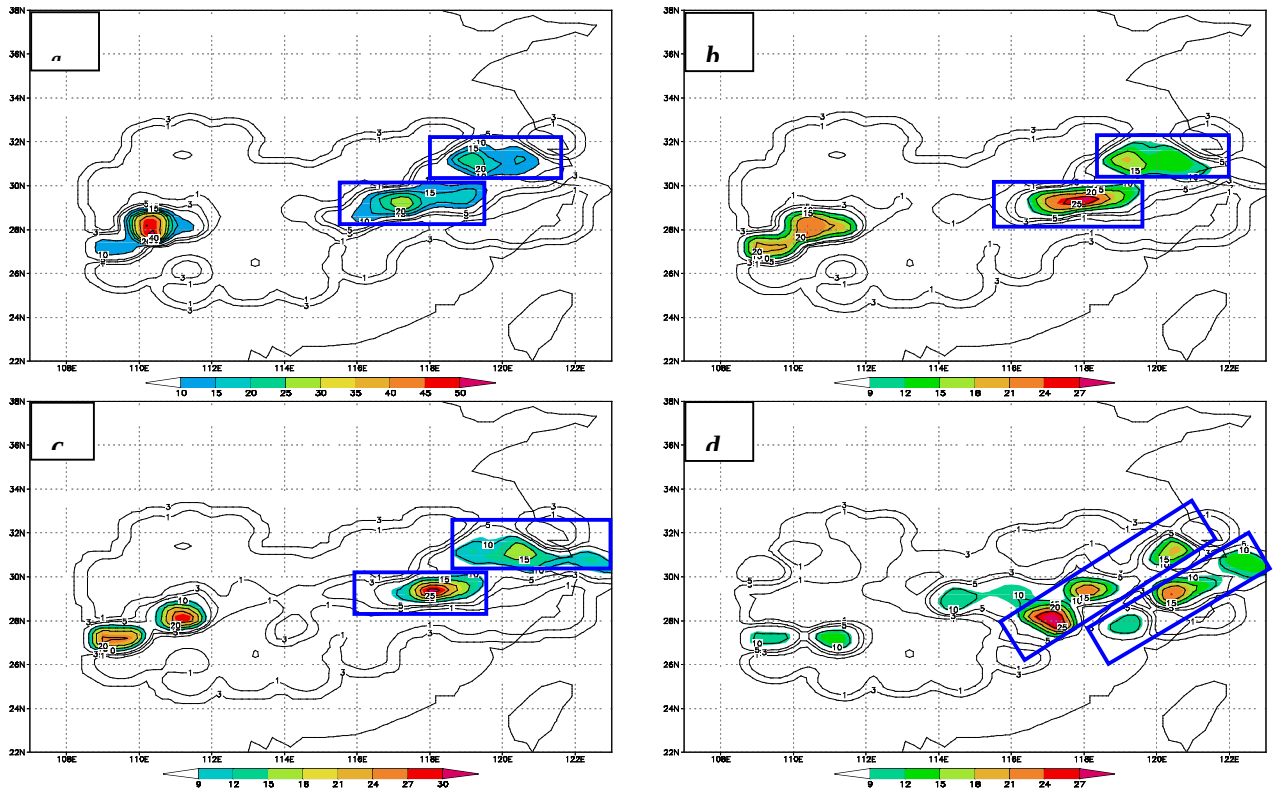

Fig 3 The observation of three-hour cumulated rainfall JUN 25 in 1999 of a) 06~08 A.M, b) 07~09 A.M, c) 08~10 A.M, d) 22~24 P.M. The shaded area denotes where the three-hour's cumulated rainfall is above 9mm. and the rectangle zone denotes the meso-scale rainbands.

and 2000 km in the meridional (perpendicular to the frontal zone).The parameterization scheme of microphysical processes includes the ice phase (Lin et al.[10]) to study the effect of the frozen process, since the observational study (Yang et al.[11]) has shown that the ice-phase particles are ubiquitous and paly a very important role in the Meiyu frontal rainstorm. The other options such as the lateral boundary condition, scheme of time integration, and so on, are the same as that of Wang et al.[12].

Some comprehensive analysis results and observation have shown that the stratification is in near neutral stabilization in rain areas but potentially unstable in warm air mass of the Meiyu front. For example, the CAPE (convective available potential energy) in the sounding diagram of Fuzhou observation station at 08:00 (L.T.) on June 23, 1999 was as much as 870 J/kg (Figure omitted), and the CAPE would be increased in the afternoon if the composite effects of both radiation- induced temperature increase and humidity increase induced by moisture advection of the southwesterly jet in low level are taken into account. Thus, in the following experiments, an ideal sounding, whose CAPE is about 3000 J/kg, is designed to include these effects. And this kind of CAPE increase is equivalent to the thermal bubble initiating for convection (Klemp and Wilhelmson 1978).

2.2 *Moist adjustment designs*

The Meiyu frontal zone is ideally designed as a transition band with clear difference in temperature and moisture. Meiyu front is supposed to be parallel to the east-west direction, and a shallow easterly wind perturbation located below the frontal zone. In addition, a cold virtual potential temperature perturbation balances the easterly wind. According to the principle of geostrophic adjustment (Rossby[13]), the moist thermal field would adjust toward the dynamic field initiated by the easterly wind. Considering the moist dynamic feature of the Meiyu front, the adjustment process is supposed to satisfy the moist thermal wind relation:

$$\frac{\partial q_v'}{\partial y} = -\frac{f_0 q_{v0}}{g}\frac{\partial u'}{\partial z} \tag{1}$$

where f_0 is the Coriolis parameter, θ_{v0} is the virtual potential temperature in reference state (θ_{v0}=300K), and g is the gravity acceleration. That means, given the easterly wind perturbation u'(zonal velocity component perturbation), its vertical shear would generate a meridional horizontal gradient of virtual potential temperature perturbation. The initial easterly wind u' is designed as the following:

$$u'(y,z) = -\frac{L-y}{2y_0}u_m\{1-\tanh[b(L-y+az-y_0)]\} \tag{2}$$

where the α , β ,u_m, L and y_0 are constants, β = 0.00002m^{-1}, α = 100, u_m = 20m/s, the maximum value of perturbation wind speed, y_0 = 800 km, and L = 2000 km are chosen. Fig.4a illustrates that there exists a center of u' situated at the northern side of the simulation domain in the low level below the frontal zone.

It should be noted that the virtual potential temperature perturbation is introduced in Eq.(1) instead of potential temperature perturbation due to the existence of water vapor. Since virtual potential temperature is neither a conventional observation nor a model predicted variable, the approximate relationship between them in the absence of condensation is expressed as the following:

$$q_v \approx q + 0.608 q_0 \cdot q_v \tag{3}$$

where θ_0 is a reference state constant (θ_0=300K). Moreover, considering the separation of variables under the ARPS model dynamic framework,

$$\begin{cases} q = \bar{q}(z) + q' \\ q_v = \bar{q_v}(z) + q_v' = q_{v0}(z) + q_v' \\ q_v = \bar{q_v}(z) + q_v' \end{cases} \tag{4}$$

where the variable with a prime is the perturbation, and the variable with a transversal above is the base state or the environment, which are determined from an ideal sounding with potential instability energy. Thus, we can obtain the following expressions:

$$q_v' \approx q' + 0.608 q_0 \cdot q_v' \tag{5}$$

$$\bar{q_v} \approx \bar{q} + 0.608 q_0 \cdot \bar{q_v} \tag{6}$$

From Eq.(1) and Eq.(5), given the distribution of moisture, the meridional horizontal gradient of potential temperature perturbation could be obtained with the restriction of the thermal wind balance. Then we can obtain the potential temperature perturbation, which is supposed to be zero at the southern boundary.

According to the main feature of moisture in the Meiyu front, an idealized water vapor mixing ratio distribution is designed, in which the cold air mass behind the frontal zone is much drier than the warm air mass in the front of the frontal zone. Therefore, the frontal zone is indeed a transition zone of water vapor. Importantly, a moisture tongue extending from the warm section comes close to the frontal zone. This moisture tongue is a very important feature of the Meiyu front, which is the water vapor source for the

cloud (rain) bands in the Meiyu front. Though being similar to the basic treatment of moisture in Wang et al. (2002), two transitional factors, γ and α in Eq.(7), are introduced in the distribution of q'_v. Such consideration leads to the following initial distribution of perturbation water vapor mixing ratio (q'_v):

$$q'_v(y,z)=\begin{cases} q_{v0}(z)\cdot(g-1) & y<y_s-D(z) \\ 0 & y_s-D(z)\le y<y_s \\ \left[-a\left(\frac{y_s-y}{d}\right)\right]\cdot q_{v0}(z) & y_s\le y<y_n \\ \left[-a-a\left(\frac{y_n-y}{y_n}\right)\right]\cdot q_{v0}(z) & y\ge y_n \end{cases} \quad (7)$$

where $q_{v0}(z)$ is the water vapor mixing ratio in the warm air mass (environmental air), y_s and y_n are the southern boundary and northern boundary of the transition zone, respectively. Moreover, α = 0.45 is a control factor of moist contrast across the front; γ = 0.75 is a control parameter of the humidity in the south of the moisture tongue. And d = 400 km is the width of the transition zone. D(z) is the southern boundary of the moisture tongue. Such distribution of the initial moisture mixture ratio can be seen from Fig.4b. It is worth noting that the moisture tongue shows a large value of q_v in the foreside of the frontal zone.

Now, we can calculate the perturbation potential temperature q' (Fig.4c) from Eq.(1), Eq.(5) and Eq.(7). In comparison with u' (Fig.4a) and q'_v (Fig.4b), it is manifested that the cold air perturbation is corresponding with drier mass and the easterly wind perturbation, while the moisture tongue is just situated on the leading edge of this cold air perturbation. Such distributions of the moist dynamic field basically agree with the results from composite synoptic analysis.

Since the Meiyu frontal zone is defined by equivalent potential temperature q_e in composite synoptic analysis, we still need to calculate q_e. With the distribution of potential temperature and water vapor mixture ratio, the equivalent potential temperature q_e can be obtained.

$$q_e \approx q\cdot\exp\left(\frac{L_v\cdot q_v}{C_p\cdot t_d}\right) \quad (8)$$

where, C_p, L_v are the specific heat at constant pressure and condensation latent of vapor respectively. q_v, t_d are the water vapor mixture ratio and dew point temperature respectively. While the dew point

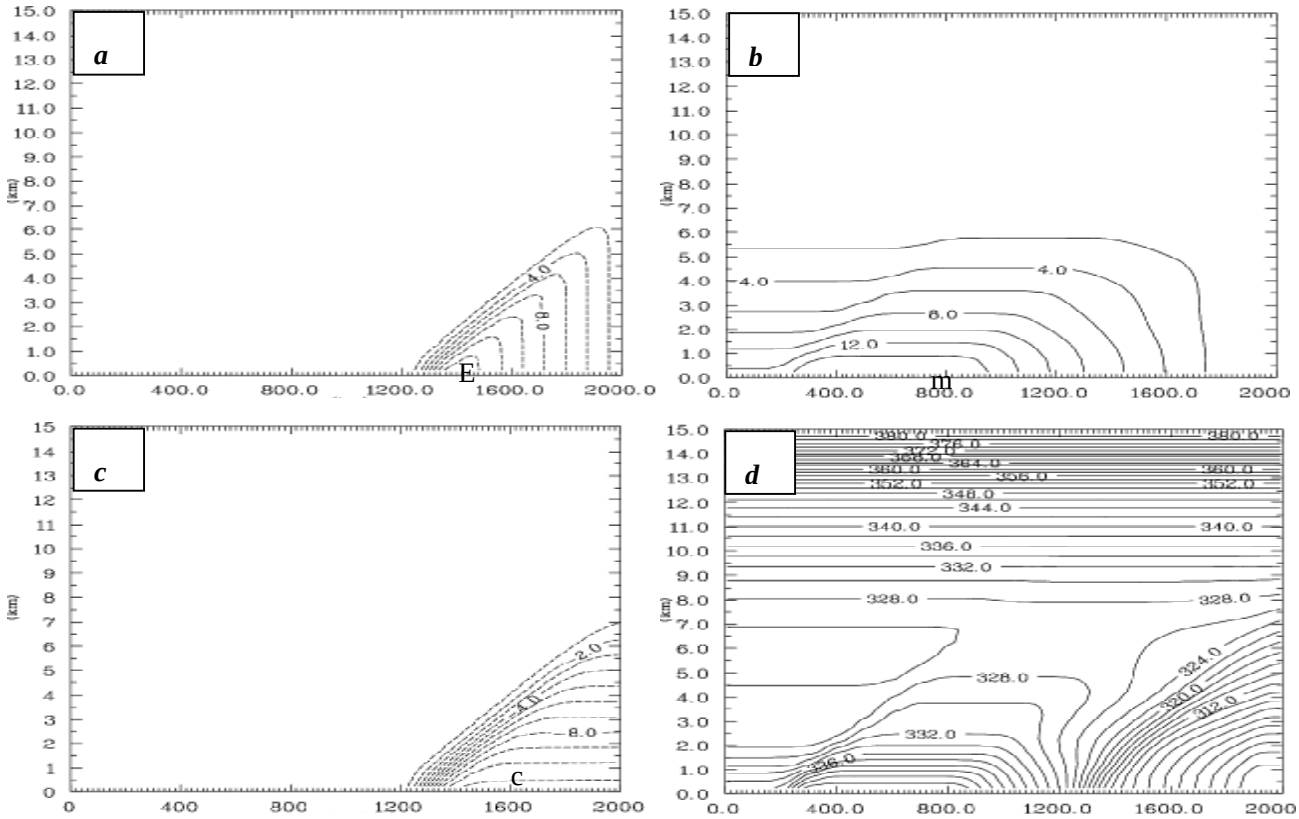

Fig.4 Initial vertical cross-section of a) zonal wind perturbation (m/s), b) water vapor mixing ratio (g/kg), c) potential temperature perturbation (K), d) equivalent potential temperature (K).And the right hand of the axis is point to the North direction.

temperature is calculated according to the enhanced experience formula (Buck[14]), in which the real pressure of water vapor can be shown as:

$$e=(a_1+b_1\cdot p)\cdot a\cdot\exp(\frac{t_d-273.15}{t_d-c}\cdot b) \quad (9)$$

where p is the total pressure, t_d is the dew point temperature (K), where a, b, c, a_1, and b_1 are the experience coefficient related with either liquid or ice water, concretely,

$$\begin{cases} a=611.21 \\ b=17.502 \\ c=32.18 \\ a_1=1.0007 \\ b_1=4.18\times10^{-8} \end{cases} \text{for liquid, and}$$

$$\begin{cases} a=611.15 \\ b=22.452 \\ c=0.6 \\ a_1=1.0003 \\ b_1=3.46\times10^{-8} \end{cases} \text{for ice.} \quad (10)$$

Running logarithm to Eq.(8), then the dew point temperature can be reduced as:

$$t_d=\frac{A\cdot c-273.15b}{A-b} \quad (11)$$

where

$$A=\ln[\frac{e}{a\cdot(a_1+b_1\cdot p)}] \quad (12)$$

However, the real pressure of water vapor can be calculated with water vapor mixture and the total pressure of moist air. Since the state equation for water vapor and the dry air can be shown respectively:

$$e=r_v\cdot R_v\cdot T \quad (13)$$

$$p-e=r_d\cdot R_d\cdot T \quad (14)$$

where R_d, ρ_d are the gas constant and density of dry air; and R_v, ρ_v are the gas constant and density of water vapor. The water vapor mixture ratio is defined as:

$$q_v=\frac{r_v}{r_v+r_d} \quad (15)$$

From Eqs.(13), (14) and (15), an alternative expression of the real pressure of water vapor can be shown as:

$$e=\frac{p\cdot q_v}{\frac{R_d}{R_v}+(1-\frac{R_d}{R_v})\cdot q_v} \quad (16)$$

Now, the real pressure of water vapor can be calculated from Eq.(16). Then, the dew point temperature can be calculated from Eqs.(12) and (11). Lastly, the initial distribution of equivalent potential temperature (Fig.4d) can be obtained from Eq.(8).

In summary, the design and calculation process of initial perturbations mentioned above is recapitulated as the following. Firstly, the easterly wind perturbation u' is designed to indicate the wind on the bottom of the North China High dam. Secondly, the virtual potential temperature perturbation q_e is calculated based on the restriction of moist thermal wind balance. Thirdly, the moisture tongue distribution is designed and the q_e is translated to q', and then the environmental potential temperature $\bar{q}^{(z)}$ is introduced to obtain the total potential temperature q. Lastly, the equivalent potential temperature q_e can be obtained after the dew point temperature is available with the aid of the enhanced Teten's formula.

2.3 *Sensitivity experiments for the profile of environmental meridional velocity*

Two experiments are designed to study the sensitivity influence of the profiles of environmental meridional velocity based on the development of the above initial perturbation as well as the generation of the meso-scale rainbands. The main features of the profiles of the environmental meridional velocity are described briefly in Tab.1.

Tab.1 Summary of sensitivity experiments on profiles of environmental meridional velocity

Test name	Profile of environmental meridional velocity	Aim
Control test	Northerly wind in high-level (maximum –8m/s); Southerly wind in low-level (maximum 10m/s)	Simulation
Sensitivity test	Uniformity of southerly wind (10m/s)	Verification

In the control test, the profile of environmental meridional velocity (Fig.5a) is based on the composite

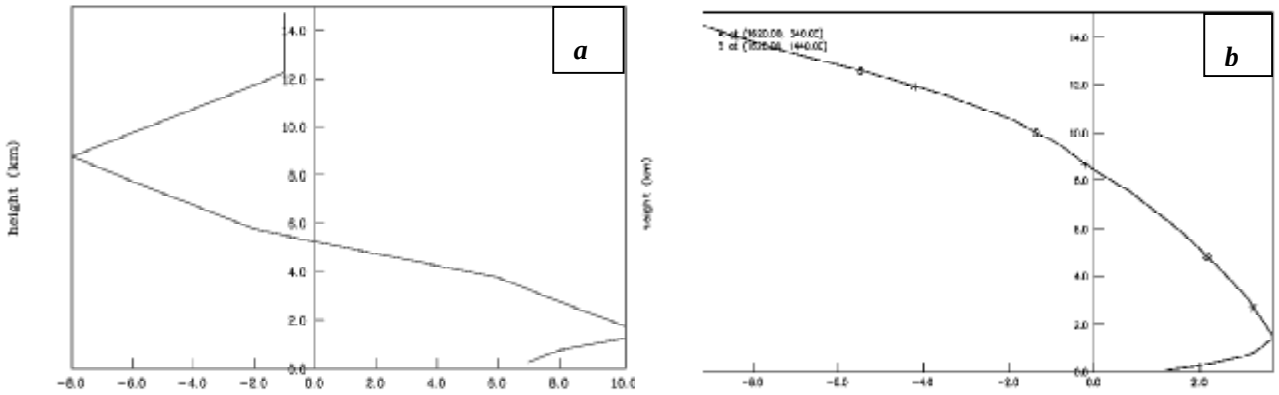

Fig 5 The profile of environmental meridional wind, a) in control test, b) in the synthesized analysis during the Meiyu period in 1999.

analysis (Fig.5b) for June 23 – July 2, 1999. However, we increase the southerly wind in low levels considering the weakening effect on the wind due to the mean across the trough. While in the high level, this weaken effect is small, so the northerly wind is not changed except for the top boundary in order to achieve integral stability. Such consideration leads to a maximum northerly wind at the 9-km level and uniform wind near the top boundary. As a whole, the vertical distribution of the environmental meridional velocity in the control test represents the main feature of the real environmental wind. Therefore, the control test simulates the development of the initial low-level easterly wind that maintains a dry and cold temperature perturbation in the typical environmental wind of the Meiyu front. Importantly, the moisture tongue is included in this initial perturbation.

While in the sensitivity test, an extremely case is considered when the South Asia anticyclone on 200 hPa is very weak. That means the northerly wind on high-level is very weak even appearing as the southerly wind as the low level. Thus the environmental wind is supposed ideally as a uniform southerly wind of 10m/s. So, the sensitivity test simulates the development of the same initial perturbation as the control test but in a kind of ideal "warm surge" by the uniform environmental southerly wind.

3 GENERATION AND MAINTAINING MECHANISM OF B MESO-SCALE RAINBANDS

3.1 *Generation and development of β meso-scale double rainbands*

When the environmental southerly wind encounters with the moisture tongue, a cloud band first generates and develops so quickly that a rain band appears at t=3.5 hours near the southern boundary of the moisture tongue both in the control test (Fig.6a) and sensitivity test (Fig.6b).

However, it is significant to compare their detailed structure. Firstly, the rain band in the control test moves northward slower than in the sensitivity test because the average southerly velocity of a low-level environmental wind is smaller than that in the sensitivity test. Secondly, there is a growing cloud band on the northern side of the rain band in the control test (Fig.6a), while this feature is not obvious in the sensitivity test (Fig.6b). Analyzing in detail the distribution of vertical velocity at the same moment is helpful for us to understand the structure difference mentioned above. In the control test, the downdraft on the north of the rain band reaches ground surface with the maximum downdraft speed of –10.8cm/s (Fig.6c), while in the sensitivity test, the downdraft in that same area extends downwards to the 2-km altitude and with the maximum downdraft speed of –5cm/s only (Fig.6d).

Such a strong downdraft flow in the control test is intensified by the convergence aloft due to the encountering of the environmental northerly wind with the northwards outflow from the top of the rain band. On the contrary, in the sensitivity test, the convergence between the environmental southerly wind and the northwards outflow from the top of the rain band is so weak (Figure omitted) that the downdraft is weaker than that in the control test. Remarkably, this downdraft flow reflects on the intensity of the dry and cold invasion from the upper level, which is manifested in the distribution of relative humidity (Fig.6e & Fig.6f). There are two separate saturated areas divided by a strong dry and cold invasion zone in the control test (Fig.6e), while those two saturated areas are still connected to each other in the sensitivity test (Fig.6f).

In addition, the distribution patterns of liquid water in the northern cloud band are similar both in the control test and sensitivity test (Fig.6g & Fig.6h).

However, an obvious difference appears in the distribution of ice-phase particles in the northern cloud band. It is very noticeable that the northern cloud band in the control test is basically composed of ice-phase particles (Fig.6i), while it is purely composed of liquid particles in the sensitivity test (Fig.6j). Therefore, the differences in microphysical structure between the control test and sensitivity test indicate that the cold temperature advection by the dry and cold downdrafts is favorable to the freezing of the supercooled liquid particles. Sequentially, the release of the latent heat in the freezing process increases the development of the northern cloud band. The aforementioned comparison between the distribution of liquid water and ice-phase water indicates that the dry and cold downdrafts play an important role in the microphysical structure of the northern cloud band.

The aforementioned analysis shows that the vertical distribution of environmental meridional velocity in the control test is favorable to the generation of the cloud band on the northern side of the main rain band. Consequently, the special structure of β meso-scale double rain bands occurs at the 6th hour in the control test simulation (Fig.7a). And the width of each rain bands is about 150 – 180 km, with 300 – 340 km distance between the axis of the rain bands. The

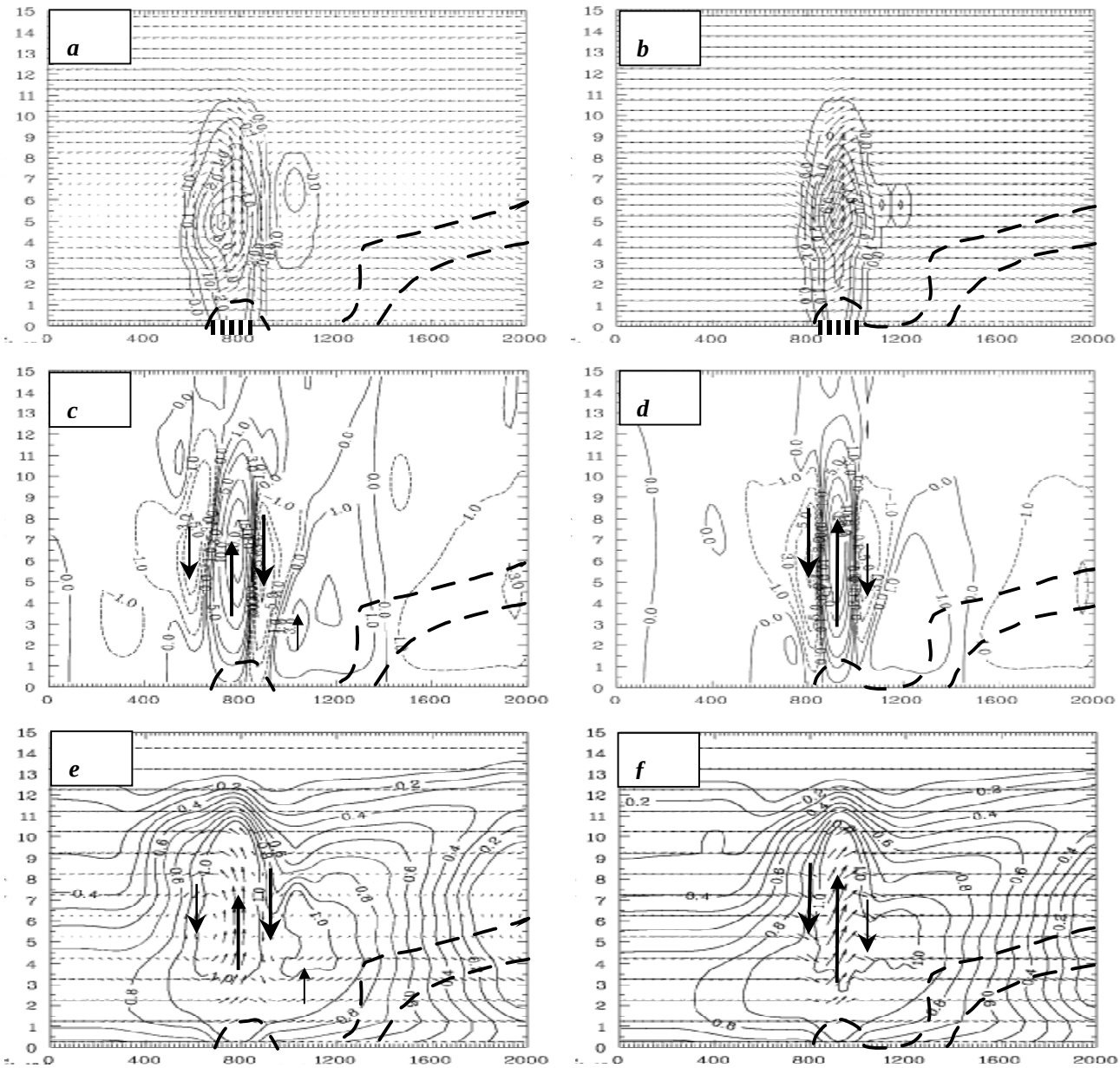

Fig.6a The contrast between control test (a,c,e,g,i) and sensitivity test (b,d,f,h,j) at t=210m of a) and b) total cloud water, " ┃ ┃ ┃ " denotes the rainbands; c) and d) vertical velocity; e) and f) relative humidity; the arrow denotes the updraft and downdraft center.

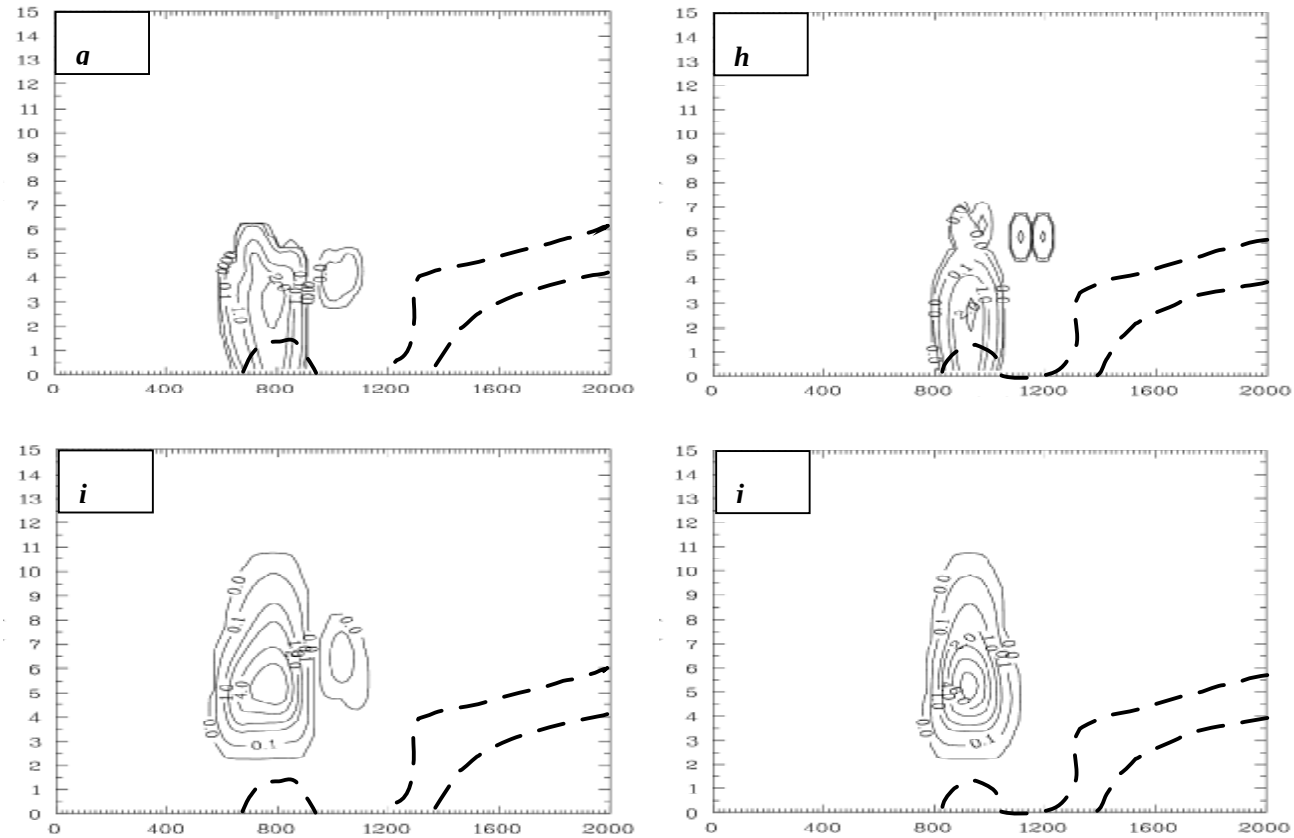

Fig 6b The contrast between control test (a,c,e,g,i) and sensitivity test (b,d,f,h,j) at t=210m of g) and h) mixture ratio of ice-phase droplets; i) and j) mixture ratio of liquid droplets. And the right-hand of horizontal axis direct the north; the coarse dashed lines approximatively denote the frontal zone.

updrafts in the southern cloud band (the main rain band), which are primarily from the convergence at low levels, divide into two outflows at the top of the cloud. One branch flows southward with the environmental current (the northerly wind), while the other branch flows northward and encounters with the environmental northerly wind to form a convergence zone. It is this convergence zone aloft that generates a narrow and strong downdraft flow, which appears as the dry and cold invasion. At the same time, after this downdraft flow reaches ground surface and encounters with the secondary circulation across the frontal zone, it generates a convergence zone in the northern side of the main rainband near the surface to maintain the cloud band at the north of the main rain band. However, in the sensitivity test, this kind of downdraft flow is weak and wide (Fig.6d), which restrains the development of the northern cloud, so that only one rainband appears (Fig.7b).

The aforementioned differences between the control test and the sensitivity test are also exhibited in the structure of vertical circumfluence. There are two "roller" positive circumfluence cells (positive circumfluence is defined as the updraft in the south while downdraft in the north, see the "C1" and "C2"in Fig.7c) in low level matching the two rainbands. And a negative circumfluence cell (negative circumfluence is defined as the updraft in the north while the downdraft in the south, see the "A" in Fig.7c) is situated on the southern side of the main rainband. Such structure of vertical circumfluence with double rainbands is in accordance with the meso-scale observations (Zhang[3]). While in the sensitivity test, there is respectively one positive and one negative circumfluence cell (see the "C1" and "A" in Fig.7d).

The release of latent heat in cloud bands caused the stability changes from potential instability to nearly neutral stability. Thus two neutral stability regions, which are corresponding to the two rainbands, appear in the control test (Fig.7e), while only one neutral stability region corresponded to a single rainband in the sensitivity test (Fig.7f).

Moreover, three maximum centers of southerly wind perturbation respectively at 1 km, 4 km, and 10 km altitude appear in the control test (see denotations "J1", "J2", and "J3" in Fig.7g), which are in good

agreement with three jets in observations of double rainbands (Zhang[3]). In contrast, there is only one jet in

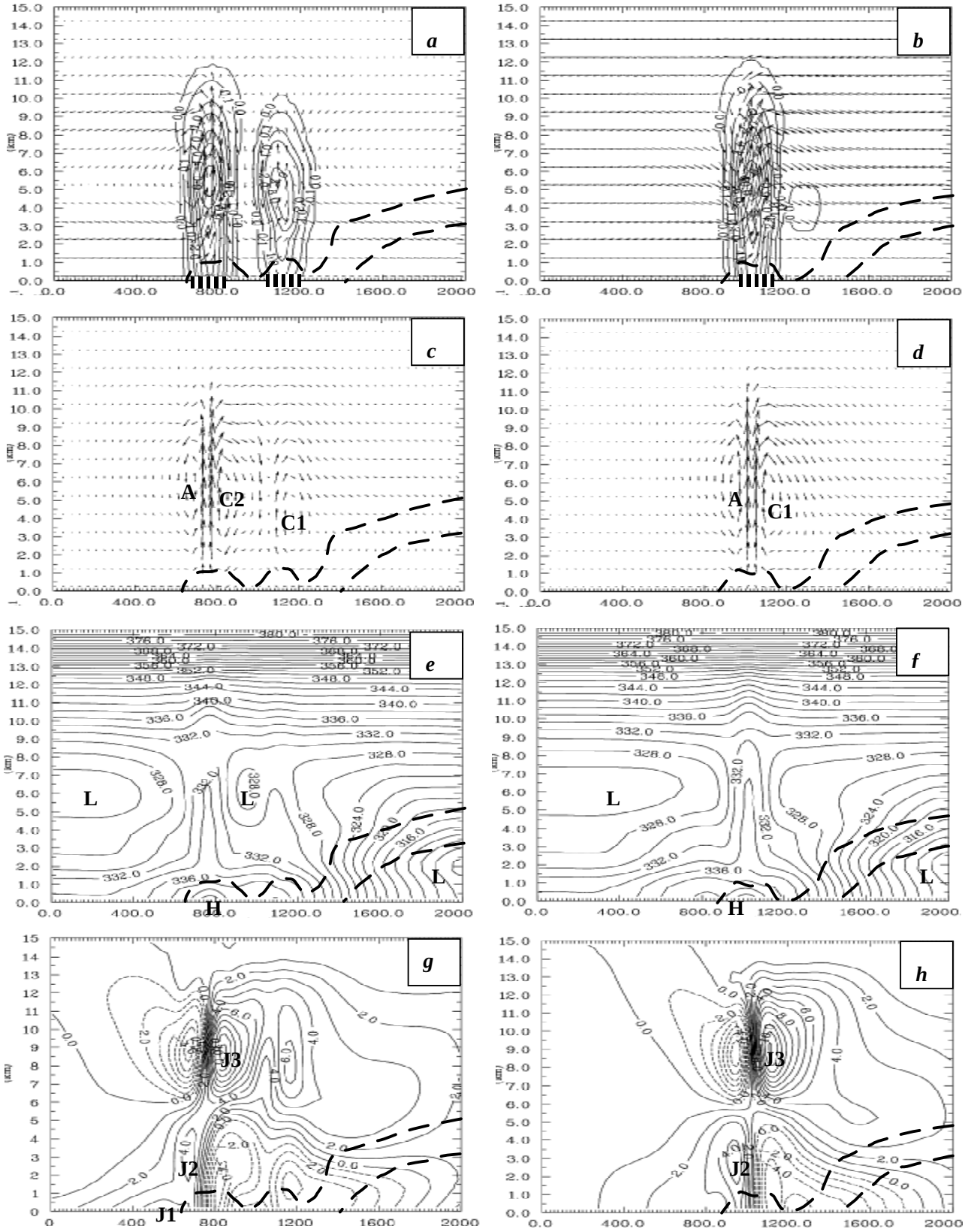

Fig 7 The contrast between control test (a, c, e, g) and sensitivity test (b, d, f, h) at t=6h of a) and b) total cloud water, " ▮▮▮▮▮ " denotes the rainbands; c and d) circumfluence of perturbation wind, "C1"and"C2" denote the positive circumfluence, "A" denote negative circumfluence; e) and f) equivalent potential temperature; g) and h) perturbation meridional velocity, "J1","J2"and "J3"denote the center of southerly wind jet. And the right-hand of horizontal axis direct the north; the coarse lines approximatively denote the front zone.

low-mid level (see denotations "J2" in Fig.7h).

In summary, in contrast with the sensitivity test, the typical vertical distribution of environmental meridional wind, especially the northerly wind aloft, plays a major role in the generation of β meso-scale rainbands in the Meiyu front and hence in their maintenance.

In addition, with the aid of the Rossby radius, Blumen[15] evaluated the wavelength of the inertial gravitational wave inspired during the geostrophic adjustment as the following:

$$l_N \approx \frac{NH}{2pf} \tag{17}$$

Here, N, H and f are respectively the Brunt-Väisälä frequency, the vertical scale of the model atmosphere, and the Coriolis parameter. And in the present paper, these parameters are chosen as the following:

$$\begin{cases} N = 1.1\times10^{-2}\,s^{-1} \\ H = 15km \\ f = 0.7511\times10^{-4}\,s^{-1} \end{cases} \tag{18}$$

Then, the wavelength of the possible inertial gravitational wave in the present paper can be evaluated as: $l = 349.62km$, which is equivalent to the distance between the rainbands in the control test.

Moreover, Benard et al.[16] analyze the wavelength of the vertical gravitation stationary wave as:

$$l_z \approx \frac{2pV}{N} \tag{19}$$

Obviously, there is a "steering layer" (Benard et al. 1992) situated on the 9-km altitude level in the distribution of environmental meridional wind in the control test. Therefore the gravitational wave is possibly "trapped" between the "steering layer" and frontal zone, which is favorable to the generation of the double rainbands. In sensitivity test, however, the "trapping" mechanism no longer exists so that only one rainband maintains.

4 SUMMARY AND CONCLUSIONS

In this study, an idealized perturbation, which is constrained by moist thermal-wind equilibrium limitation in order to be in thermodymical agreement with the "surge flow conceptual model" for typical Meiyu frontal structure, is designed to examine the structure of meso-scale rainbands, especially the generation and maintenance mechanism behind the β meso-scale double rainbands in the Meiyu front. And the sensitivity contrast experiments on the vertical distribution of the environment meridional wind is implemented using the non-hydrostatic, full-compressible storm-scale model that includes multi-phase schemes of cloud microphysical parameterization.

The numerical results of comparing the control experiment with the sensitivity numerical experiment show that the cool and dry downdraft invading that is strengthened by the environmental upper-level northerly wind plays a major role in the generation of the β meso-scale double rainbands. Firstly, when the downdraft approaches ground, it encounters with the secondary circulation across the frontal zone and generates a convergence zone in the northern side of the main rainband near surface to maintain the cloud band at the north of the main rain band. Importantly, the cold temperature advection by the dry and cold downdraft is favorable to the freezing of the super-cooled liquid particles. Then, the release of the latent heat in the freezing process increases the development of the northern cloud band.

Moreover, the intensity and scale of the dry and cool downdraft invading are related to the intensity of the second circumfluence induced by mass adjustment when the acceleration of the westerly jet aloft occurs. Following this opinion, we can respectively sum up the conceptual model for the generation of double and single rainbands (Figure omitted). The initial states are the same except for the distribution of the environmental meridional velocity (Figure omitted). The main development process are also similar, such as the generation of the cloud band in the moisture tongue, the secondary circulation across the frontal zone, and the appearance of the westerly wind perturbation above the frontal zone (Figure omitted), which means the strengthening of the high level westerly jet over the East Asia. However, the intensity of the secondary circumfluence, which is induced by the mass adjustment to the strengthening of the high level jet (Gao et al.[17]), is obviously different in the contrary environmental meridional velocity. For instance, in the control test, the northerly winds aloft enhance this secondary circumfluence so that a narrow and strong cold downdraft invading generates on the northern side of the main rainband. Accordingly, the moisture tongue is separated into two parts corresponding with two rainbands (Figure omitted). In the sensitivity test, however, the southerly winds aloft do not enhance the secondary circumfluence; therefore, the downdrafts invading on the northern side of the main rainband are weak and widely distributed. Since these weak and wide downdrafts restrain the development of new cloud band on the northern side of the main rainband, only a single rainband maintains and the moisture tongue

keeps well as a whole (Figure omitted).

In addition, the wavelength of a possible inertial gravitational wave in the present study is equivalent to the distance between the rainbands in the control test. This result indicated that a positive feedback mechanism between inertial gravitational wave and convection exists. Moreover, the "trapped" mechanism in the control test is also in favor of double rainbands. It is under investigation.

Acknowledgement The authors would like to thank Prof. Xue Ming[9] (Center for Analysis and Prediction of Storm, University of Oklahoma, USA) for providing the code of ARPS.

REFERENCES:

[1] Tao, Shi-yan, Ding Yi-hui, Zhou Xiao-ping. Research on heavy rainfall and severe convective weather [J]. Scientia Atmospherica Sinica, 1979, 3: 227- 238.
[2] TAO Shi-Yan. The Heavy Rainfall in China [M]. Beijing: Science Press, 1980.
[3] ZHANG Bing-chen. Research on Heavy Rainfall of Meiyu Rront in Yangtze River [M]. Beijing: Meteorological Press, 1990: 1-269.
[4] LI Zi-fang, GE Liang-yu, FU Mei-juan. Spatial structure of Meiyu front and evolution of related precipitation- caused front [J]. Journal of Nanjing Institute of Meteorology, 1995, 18: 588-592.
[5] TAO Shi-yan, NI Yun-qi, ZHAO Si-xiong. Research on the Generation Mechanism and Prediction of the Summer Heavy Rainfall in China [M] Beijing: Meteorology Press, 2001:1-184.
[6] BEI Nai-fang. Diagnose and simulation study on mesoscale system of the heavy rainfall prediction in July 1998 [D]. Dissertation of the Institute of Atmospheric Physics, Chinese Academy Sciences. 2000: 1-274.
[7] WU Rong-sheng. Meiyu frontogenesis and accompanying convections[C]//Proceedings of the 25th Academic Conference of the Chinese Meteorological Society, Beijing: Meteorological Press, 2002: 14-20.
[8] KLEMP J B, WILHELMSON R B. Simulation of right-hand left-moving storms produced through storm splitting [J]. J. Atmos. Sci., 1978, 35: 1097- 1110.
[9] XUE Ming, et al. ARPS Version 4.0 User's Guide [R]. Center for Analysis and Prediction of Storm. 1995: 380.
[10] LIN Y L, FARLEY R D, ORVILLE H D. Bulk parameterization of the snowfield in a cloud model [J]. J. Climate Appl. Meteor. 1983, 22: 1066-1092.
[11] WANG Chun-ming, WU Rong-sheng, WANG Yuan. Interaction of diabatic frontogenesis and moisture processes in cold-frontal rain-band [J]. Adv. Atmos. Sci., 2002, 19: 544-561.
[12] YANG Jing, WANG Peng-yun, YANG Shao-zhong. Observation and analysis on the micro- physics structure of precipitation cloud in Meiyu front [J]. Meteorological Monthly, 2000, 28: 3-8.
[13] ROSSBY C G. On the mutual adjustment of pressure and velocity disturbances in certain simple current systems. Part II [J]. J. Mar. Res., 1938, 27: 239-263.
[14] BUCK A L. New equations for computing vapor pressure and enhancement factor [J]. J. Appl. Meteor., 1981, 20: 1527-1532.
[15] BLUMEN W. Geostrophic adjustment [J]. Rev. Geophys. Space. Phys., 1972, 10: 485-528.
[16] BENARD P, REDELSPERGER J L, Lafore J P. Nonhydrostatic simulation of frontogenesis in a moist atmosphere. Part I: General description and narrow rainbands [J]. J. Atmos. Sci., 1992, 49: 2200-2217.
[17] GAO Shou-ting, TAO Shi-yan. The lower layer frontogenesis induced by the acceleration of upper jet stream [J]. Scientia Atmospherica Sinica, 1991, 15(2): 11-22.